2519铝合金角接结构的搅拌摩擦焊

马慧坤， 贺地求， 刘金书
(中南大学 机电工程学院，长沙 410083)

马慧坤

摘 要：利用自行研制的搅拌摩擦焊机采用一种搅拌摩擦焊外侧角接的新方法对厚度为22 mm的2519铝合金进行了角接焊接试验，并对焊缝的微观组织、硬度等进行了分析. 分析了搅拌针断裂原因及得出其断裂方式为剪切断裂. 结果表明，搅拌摩擦焊外侧角接焊接的方法能够有效地进行角接焊接；合理的焊接工艺和搅拌针形状是焊接的关键；旋转频率在30～40 rad/s，焊接速度在90～120 mm/min的范围内都可以获得良好的接头外观.

关键词：搅拌摩擦焊；外侧角接；2519铝合金
中图分类号：TG453 **文献标识码**：A **文章编号**：0253－360X(2011)08－0073－04

0 序 言

搅拌摩擦焊[1](friction stir welding，FSW)作为一种新型焊接技术，是由英国焊接研究所(TWI)于20世纪90年代初发明的一种固态焊接方法. 近年来，随着航天、军工和汽车等行业对熔焊性差的高强铝合金等特殊材料的需求量不断增加，推动了搅拌摩擦焊接技术的发展，并成为21世纪国内外研究的热点. 目前对搅拌摩擦焊平板的对接焊接研究得比较多，0.8～75 mm厚的铝合金都可以实现搅拌摩擦焊接[2]. 实际工程应用中大多数工程焊接结构采用型材或板材以角接方式构成，但由于搅拌摩擦焊主要是由轴肩与被焊接面摩擦产生热量，因此受到搅拌摩擦焊结构限制，不能直接进行角接焊接. 美国的Trapp等人[3]发明了一项L和T形角接焊接时的专利. 日本的Katsuaki等人[4]为了解决用搅拌摩擦焊焊接工字型材料，采用了辅助的三角垫块来填充焊接部位. 日本一项发明专利[5]提出一种从角接缝内侧(夹角＜180°一侧)设一具有三角形断面的工艺垫块，填平焊接内夹角，焊接时搅棒穿过工艺垫块，进入焊件接缝，台肩则与垫块表面摩擦，实现角接焊接. 文中采用一种新型的外侧角接焊接的方法，对2519铝合金进行了搅拌摩擦焊角接进行了焊接. 试验表明，此方法可以对任意角度的焊件进行搅拌摩擦焊焊接，在工程中具有很高的实际应用价值. 2519铝合金是20世纪80年代美国开发的一种高强、高韧铝合金. 文中利用搅拌摩擦焊外侧角接焊接的方法对2519铝合金厚板成功地进行了角接焊接，并进行了金相分析和硬度测试.

1 焊接方法

利用在待焊接件角部外侧镶拼辅助工艺垫块，在构成任意角度的角接焊缝顶部形成平面结构，解决搅拌摩擦焊工艺对焊接部位的特殊要求. 该角接焊接法能从封闭或半封闭角接构件外侧焊接. 如图1所示，1和5为待焊件，2和4为工艺辅助垫块，3为搅拌头. 设待焊件1，5的角接半角为α，其实际焊接的夹角为2α，焊接后，把1和5焊接起来. 将垫块2，4加工成角度为β的坡口，并使$\alpha+\beta=90°$. 该辅助垫块的主要作用是通过角度的拼接，形成搅拌摩擦焊所需的台肩摩擦平面，把成角度的搅拌摩擦焊转化为平板对接焊，通过搅拌头3与2，4组成的表面摩擦，把产生的热传递给实际待焊件. 搅拌头3通过与垫块2，4组成的平面摩擦产生热量传递给焊接板上，使焊接板在一定的区域金属塑化达到可以搅拌的状况，然后在其搅棒的搅拌作用下完成搅拌摩擦焊. 焊完后去除工艺垫块2和4，即可得到搅拌摩擦焊角接头.

2 焊接材料与试验

试验中采用的2519铝合金主要成分及力学性

收稿日期：2010－07－12
基金项目：国家自然科学基金资助项目(500675228)

能如表 1 与表 2 [6] 所示.

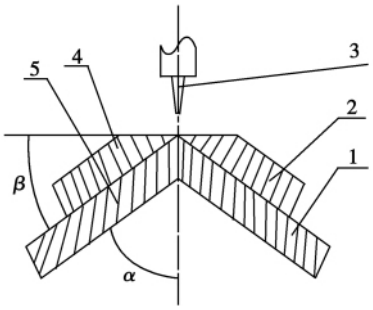

图 1 搅拌摩擦焊角接外侧焊工作原理图

Fig. 1 Working principle of fillet welding

表 1 2519 铝合金的化学成分(质量分数,%)

Table 1 Chemical constitution of 2519 alloy

Cu	Mg	Mn	Zr	Al
5.80	0.22	0.28	0.21	余量

表 2 2519 铝合金的力学性能

Table 2 Tensile strength of 2519 alloy at room temperature

抗拉强度 R_m/MPa	屈服强度 R_{eL}/MPa	断后伸长率 A(%)
460	398	12.0

试验采用自行研制的搅拌摩擦焊机和夹具对 22 mm 厚的 2519 高强度铝合金进行焊接,焊接角度为 120°,焊缝深约为 25 mm. 搅拌头参数为轴肩 35 mm,搅拌针直径 12 mm,底部直径调整变化,长度 23 mm,夹具采用自制专用角接焊接夹具.

试验中在不同形状搅拌针与旋转频率和进给量之间进行组合匹配,利用 Raytek 非接触式红外测温仪对轴肩温度进行实时监测,用 POLYVAR - MET 光学金相显微镜对焊接接头进行金相分析,在 HVA - 1000 维氏硬度计上进行硬度测试.

3 试验结果与分析

3.1 焊接工艺分析

搅拌摩擦焊这种新型的固相连接方法再焊接过程中不同的工艺参数得到的接头焊接质量有很大的差异,在厚板焊接时工艺参数影响尤为明显. 影响搅拌摩擦焊接头质量的主要参数有轴肩直径大小、搅拌针形状以及旋转频率和焊接速度.

经过大量的试验证明,搅拌头参数为轴肩 35 mm,搅拌针直径 12 mm,底部直径 3.5 mm,长度 23 mm,旋转频率在 30 ~ 40 r/s,焊接速度在 90 ~ 120 mm/min 的范围内都可以获得良好的接头外观.

试验中发现,不同形状的搅拌针对能否获得良好的焊缝质量有至关重要的作用. 搅拌针底部直径过小时,如果焊接工艺不当靠近搅拌针底部因为搅拌针直径过细经常会发生剪切断裂. 搅拌针底部直径过大或者旋转频率过低时,焊缝区域材料流动不充分阻力过大,搅拌针会被从靠近轴肩的地方剪断. 多次重复试验证实,采用底部直径 3.5 mm 的搅拌针焊接效果比较好.

因为是厚板角接焊接,所以当旋转频率低于 20 r/s 时,焊接时温度过低,轴肩温度低于 220 ℃,材料粘度过大,流动不充分,所受阻力较大,底部容易出现空洞,同时搅拌针也容易断裂.

3.2 焊缝性能分析

3.2.1 焊缝微观组织

由于国内尚无角接焊接拉伸的有关标准以及角接焊接试样拉伸试验比较困难,所以暂不对 2519 铝合金摩擦搅拌焊角接焊接接头进行力学性能测试.

在旋转频率 36.67 r/s,焊接速度为 92.56 mm/min的焊接工艺条件下对 22 mm 厚的 2519 铝合金焊接. 用线切割机横向切割取样取焊缝的横截面制作金相试样,对断面用碳化矽砂纸(400 ~ 2000 号)进行粗磨和精磨,然后再在抛光机上用绒布抛光到镜面水平. 可以看到明显的焊缝区域的整体形貌,最后再经过化学腐蚀处理. 采用此焊接方法焊接试样的微观组织如图 2 所示. 从图 2 可以看到试样截面搅拌摩擦焊接区与母材区的明显交界,呈现“U”字形特征,焊缝中宏观组织的光泽存在明暗差异,存在以焊缝中心大致对称较明显的界线,这是由焊缝中组织的构成,形貌,走向等的变化引起的,据此可将焊缝分为三个区: 焊核区 WNZ(weld nugget zone),热力影响区TMAZ(thermo-mechani-

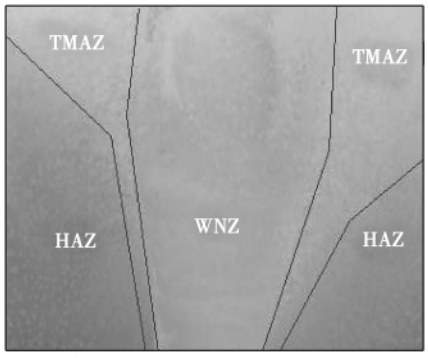

图 2 2519 铝合金厚板角接焊接焊缝宏观横截面形貌

Fig. 2 Cross-section of FSW by fillet welding

cally affected zone),热影响区 HAZ(heat affected zone).

图 3 ~ 图 6 分别是母材区、焊核区、热力影响区、热影响区四个区的金相微观组织. 焊核区位于焊缝的中间部位,底部形状大小与搅拌头实际尺寸比较接近,上部靠近轴肩部分由于受轴肩和搅拌针的机械搅拌以及剧烈摩擦产生的局部高温,组织发生了动态再结晶,变成了比母材组织更为细小的等轴晶组织,见图 4.

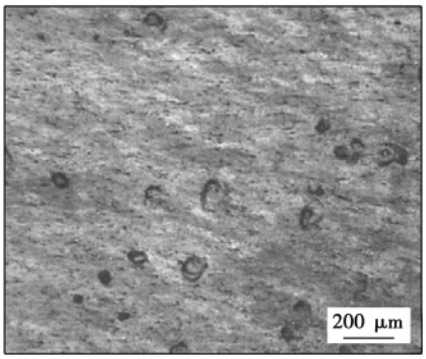

图 3　母材金相微观组织

Fig. 3　Microstructure of base metal zone

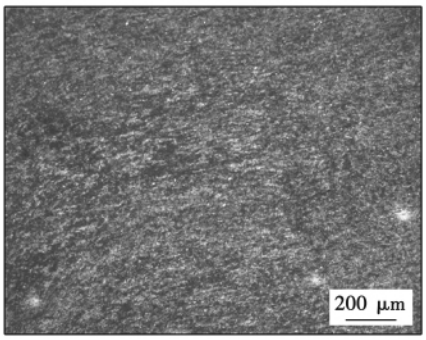

图 4　焊核区金相微观组织

Fig. 4　Microstructure of weld nugget zone

热力影响区由于搅拌头的搅拌作用不充分不能使呈轧制状的母材组织完全破碎,而是在搅拌旋转作用力和焊接进给力的双重作用下发生热剪切,产生较大的晶粒变形. 但是该区域温度较焊核区低,没有达到再结晶温度,不能发生类似焊核区的再结晶过程. 热力影响区由于受到焊接热循环作用,晶粒有一定程度长大粗化,与母材组织无明显区别如图 5 所示. 图 6 热影响区是没有受到搅拌头作用的区域,但是在焊接过程中由于剧烈的摩擦产生大量的热量,在热循环作用下导致该区域基材组织相比母材发生了粗化.

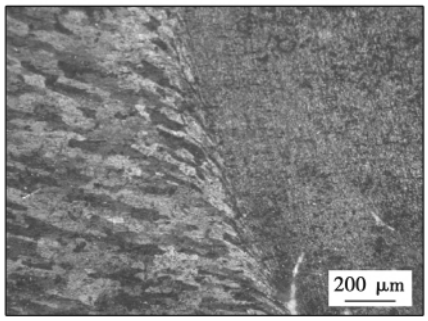

图 5　热力影响区金相微观组织

Fig. 5　Microstructure of thermo-mechanically affected zone

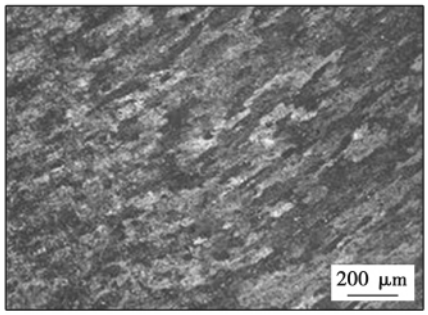

图 6　热影响区 HAZ 金相微观组织

Fig. 6　Microstructure of heat-affected zone

3.2.2　焊缝硬度分析

焊接后,对截取好的试样进行研磨和抛光,用 HVA－1000 维氏硬度计在焊缝横断面 10 mm 深处进行硬度检测,结果如图 7 所示. 图中 A 区为焊核区,B 区为热力影响区与热影响区,C 区为母材区,断面硬度呈 U 形分布. 从图 7 中可知,硬度分布从热影响区到焊核区硬度值都出现不同程度降低,焊核区力学性能下降最大,硬度下降了大约 40%.

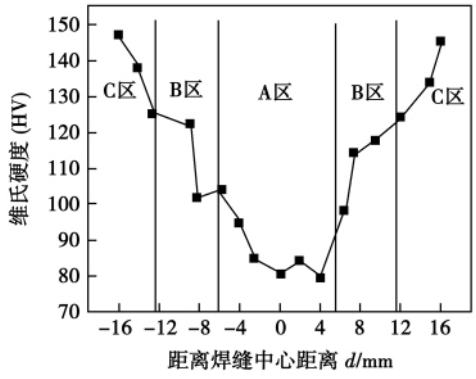

图 7　焊接接头硬度分布

Fig. 7　Microhardness distribution in 2519 aluminum alloy joint

在焊核区由于距离搅拌头较近,受搅拌头高速

旋转的搅拌作用比较强烈，局部温度比较高，基材组织完全被破坏，发生完全的动态再结晶，因此力学性能下降最多.

4 结 论

(1) 采用合理的工艺参数和搅拌头形状，可以用搅拌摩擦焊外侧焊接的方法进行外侧角接焊接.

(2) 搅拌针的形状对能否进行有效的焊接至关重要，底部直径过大或过小都容易发生断裂，过大容易在搅拌针靠近轴肩的根部断裂，过小容易在靠近搅拌针底部断裂，断裂形式均为剪断.

(3) 采用此方法得到的金相组织与厚板焊接时金相组织相似，有明显的区域分布，分别为焊核区、热力影响区、热影响区. 其硬度值在焊核区最低，相比母材下降了约 40%.

参考文献:

[1] Thomas W M T, Nicholas E D, Needham J C, *et al*. Friction stir butt welding [P]: UK, 9125978.8. 1991 - 01 - 12

[2] 栾国红. 搅拌摩擦焊在中国的发展 [J]. 电焊机, 2004(增刊), 100.
Luan Guohong. Development of friction stir welding in China [J]. Electric Welding Machine, 2004, S1: 100.

[3] Trapp T J, Stotler T, Skilliter M. Friction stir welding of corner configuratiaons [P]. United States Patent, US6,676,008 B1, 2004 - 01 - 13.

[4] Katsuaki T, Masatoshi E. Corner joining method by friction stir welding [P]. Japan: 2000147775, 2000 - 05 - 19.

[5] Kazutaka O, Masayuki D, Masahiko S, *et al*. Membrane for corner friction stir welding member welding method for the same [P]. Japan: 2001191157, 2001 - 06 - 25.

[6] 李慧中，张新明，陈明安，等. 2519 铝合金时效过程的组织特征 [J]. 特种铸造及有色合金. 2005, 25(5): 273 - 275.
Li Huizhong, Zhang Xinming, Chen Ming'an, *et al*. Microstructure characteristics of aged 2519 aluminum alloy [J]. Special Casting & Nonferrous Alloys, 2005, 25(5): 273 - 275.

作者简介: 马慧坤，男，1977 年出生，博士研究生. 主要从事搅拌摩擦焊工艺及机理方面的研究. 发表论文 3 篇. Email: liujsmhk@126.com.

improved. The best wettability and mechanical property of soldered joint is obtained when the content of Pr is 0.05 wt. %. Moreover, when the content of Pr is exceeded 0.1 wt. %, plenty of Sn-Pr compounds are found in the Sn-9Zn solder, which lead to the growth of whiskers.

Key words: rare earth Pr; wettability; microstructure; mechanical property; Sn whisker

Characteristics analysis of combined plasma arc based on sequential coupling method of physics environment approach

MENG Jianbing[1], XU Wenji[2], DONG Xiaojuan[1], YIN Zhanmin[1] (1. Shandong Provincial Key Laboratory of Precision Manufacturing and Non-traditional Machining, Shandong University of Technology, Zibo 255049, China; 2. Key Laboratory for Precision and Non-traditional Machining Technology of Ministry of Education, Dalian University of Technology, Dalian 116024, China). p 57 - 60

Abstract: According to the features of combined plasma arc and the theory of magnetic fluid dynamics and electromagnetics, which exists a coexistence of transferred arc and non-transferred arc and an interaction of electric field, magnetic field, thermal field and flow field, a three-dimensional mathematical model was developed. The effects of working current and gas flow on the distribution of jet temperature of the combined plasma arc were analyzed by finite element software ANSYS and sequential coupling method. The results show that the simulation value with this model is consistent with the measured value.

Key words: physics environment; sequential coupling method; combined plasma arc; performance evaluation

Motion control algorithm of cutting robot for ellipsoidal pressure vessels opening

LIU Tao[1], WANG Zongyi[1], DU Hongwang[1], XIE Jujun[2] (1. College of Automation, Harbin Engineering University, Harbin 150001, China; 2. Daqing Oilfield Engineering Co., Ltd., Daqing 163712, China). p 61 - 64

Abstract: According to ellipsoidal pressure vessels opening and cutting groove, a special four degrees of freedom cutting robot was developed. The mechanical structure and the working principle were introduced, and the intersecting line mathematic model of ellipsoidal shells opening in polar coordinates was established by using space analytic geometry. The groove angle calculation formula and four-axis motion control algorithm during groove cutting were derived, and ideal movement trajectory was obtained through linear interpolation algorithm. In order to eliminate the disturbances of location error and vessel distortion, teaching compensation algorithm based on theory calculation was proposed to correct robot motion trajectory. The practical application results illustrated that opening and groove cutting can be realized with the special cutting robot, and the cutting quality meets the technology requirements.

Key words: utting robot; groove cutting; intersecting line calculation; interpolation

Influence of Ag element in 62Sn36Pb2Ag on properties of AgCu/SnPbAg/CuBe solder joint

DING Ying[1], SHEN Kun[1], ZHANG Ran[2] (1. Beijing Institute of Control Engineering, Beijing 100190, China; 2. College of Mechanical Engineering and Applied Electronics Technology, Beijing University of Technology, Beijing 100124, China). p 65 - 68

Abstract: 62Sn36Pb2Ag solder and 63Sn37Pb eutectic solder were adopted to join the AgCu alloy bulk and CuBe alloy sheet. The mechanical properties and the relative microstructure for both solder joints were compared and analyzed by the experimental studies. The influence mechanism of Ag element in 62Sn36Pb2Ag on the properties of the AgCu/SnPbAg/CuBe solder joint was elaborated in detail accordingly. The results show that the Ag element in the solder changes the wetting behavior and benefits the less voids, the dispersed distribution of the Ag_3Sn particles contributes the dislocation clinching and results in the higher solder joint strength, and the nearly saturated state of Ag content in the solder joint under the soldering temperature prevents the brittle Ag3Sn phase enriching near the interface and gives the ideal microstructure of the solder joint.

Key words: 62Sn36Pb2Ag solder; Ag-based alloy; soldering

Analysis of current-carrying region of TIG arc with low-disturbing electrostatic probe

LI Yuanbo, ZHU Liang (State Key Laboratory of Gansu Advanced Non-ferrous Metal Materials, Lanzhou University of Technology, Lanzhou 730050, China). p 69 - 72

Abstract: For understanding the character of TIG arc current-carrying region and ascertaining the range of current-carrying region, a low-disturbing electrostatic probe was developed to measure the potential of probe in floating condition and the current of probe with bias voltage in various sections along the axial direction of arc. The results show that it can get the ion saturated current by probe with negative bias voltage and the electron saturated current by probe with positive bias voltage. And then the half widths of the ion saturated current peak and the electron saturated current peak can represent the radius of current-carrying region and arc including peripheral negative ion region respectively. Both of the range of current-carrying region and arc increase into widest near anode from cathode to anode along the axial direction of arc. In addition, it is found that the effect on probe caused by peripheral negative ion region of arc can reduce the potential of probe in floating condition. This effect can be neglected when the exposed length is decreased into 5 - 6 mm.

Key words: low-disturbing electrostatic probe; current-carrying region; arc; exposed length of probe

Friction stir fillet welding of 2519 aluminum alloys

MA Huikun, HE Diqiu, LIU Jinshu (College of Mechanical and Electrical Engineering, Central South University, Changsha 410083, China). p 73 - 76

Abstract: Using a new method of fillet welding, the friction stir outer fillet welding, we welded the 2519 high-strength aluminum alloy plate 22 mm thick, and analyzed the microstructure and microhardness distribution of fillet welding joint and the reason of the fracture of welding stirring pin, which the type of fracture is shear fracture. The results show that the welding method can effectively carry on fillet welding; the reasonable

welding process and welding stirring pin shape are the key of high-quality fillet welding joint. When the rotation speed is 30 – 40 rad/s and the welding speed is 90 – 120 mm/min, we can get a high-quality weld appearances.

Key words: friction stir welding; outer fillet welding; 2519 aluminum alloys

Ultra-high cycle fatigue behaviors of Q345 bridge steel welded joint FANG Donghui[1], LIU Yongjie[2], CHEN Yiyan[3], WANG Qingyuan[2] (1. Department of Civil Engineering & Architecture, College of Jincheng, Sichuan University, Chengdu 610065, China; 2. Department of Mechanics and Engineering Science, Sichuan University, Chengdu 610065, China; 3. Shenzhen Municipal Design & Research Institute, Shenzhen 518029, China). p 77 – 80

Abstract: The high cycle and ultra-high cycle fatigue properties of Q345qC base metal and circular butt weld joint were studied by using the ultrasonic fatigue testing technique. The experimental results show that during $10^5 - 10^9$ cycles, the fatigue strength of welded joint is much less than that of base metal, and both their S-N curves descend continuously. Fracture can still occur on base metal beyond 10^7 cycles and on welded steel beyond 5×10^6 cycles. The observation of fracture surface shows cracks mainly initiate from welded toes at fusion area or geometric discontinuity at the surface in welded steel. Furthermore, fatigue failure occurs at the geometric discontinuity area in the high stress regime but occurs at welded toes in the low stress regime.

Key words: ultra-high cycle fatigue; welded joint; ultrasonic fatigue test; S-N curve; fracture surface

Numerical simulation of dynamic laser melting behavior and temperature field on cast iron surface YI Peng, LIU Yancong, SHI Yongjun, JIANG Hao (College of Mechanical and Electronic Engineering, China University of Petroleum, Dongying 257061, China). p 81 – 84

Abstract: For explicitly understanding the thermo-mechanism of laser melting process on cast iron, a validated dynamic three-dimensional numerical modal for this process was established by taking into account the thermal physical parameters and latent heat of the material. The temperature field and the relationships between different process parameters were studied with this model, and the simulation results were in accordance with the experimental results. The results indicate that the penetration depth of the laser melting process on cast iron is grater than that on the steel. The large temperature gradients inside and outside the molten pool are dominated by the depth and width components respectively. A larger temperature gradient is gained through reducing scan speed and spot size. The pool is shrunk by the increase of scan speed and spot radius; the solidification speed is raised with the increase of laser scan speed and reduction of the spot size.

Key words: laser melting process; cast iron; numerical simulation; transient temperature field; molten pool

Microstructure and properties of Er-containing aluminum alloy TIG weld joints JIN Likun[1], LI Xiaoyan[1], HE Dingyong[1], JIANG Jianmin[1], YANG Dongxia[2], NIE Zuoren[2] (1. College of Materials Science and Engineering, Beijing University of Technology, China; 2. New Functional Materials Key Laboratory of Ministry of Education, Beijing University of Technology, Beijing 100124, China). p 85 – 88

Abstract: To study the strengthening effect and mechanism of Er element on the weld, the remelting welding of Al-Mg alloy with Er was adopted, and the organizational structure and mechanical properties of the joint were observed. The results show that there is primary Al_3Er phase precipitation on the grain boundaries in weld, but the quantity of it is fewer than that of in the base material, and the precipitation doesn't form a continuous ring. The secondary Al_3Er precipitation also can be found in the welding, but the precipitation phase quantity is very few. Er elements will presence in the solid solution or segregation way. The strength of Er element on the weld joint is mainly based on the primary Al_3Er to refine the grain. The effect of the secondary phase on the weld joint is small, and so the weld joint mechanical properties decrease evidence. The tensile strength of welded joints is 297 MPa, and the strength coefficient of welded joints is 72% of base material. Tensile fracture position is mainly in the center of the weld and near the fusion zone.

Key words: primary phase; secondary phase; fine-grain strengthening; precipitation strengthening

Mathematical model based on MATLAB for intersection seam of sphere and tube ZHAO Jie[1,2], HU Shengsun[1,2], SHEN Junqi[1,2], CHEN Changliang[2], DING Wei[1] (1. Tianjin Key Laboratory of Advanced Joining Technology, Tianjin University, Tianjin 300072, China; 2. School of Materials Science and Engineering, Tianjin University, Tianjin 300072, China). p 89 – 92

Abstract: The welding process of complex space curve, such as intersection seam of sphere and tube, is difficult in the field of welding automation, and the construction of a mathematical model of intersection seam is a prerequisite for the welding process. After a mathematical model of intersection curve of sphere and tube is established with MATLAB software, by further analysis, the intersection curve can be simplified to plane curve. By considering the thickness effects of the sphere, some amendments to the model of J-shaped groove weld are made by increasing $\triangle D$ and $\triangle d$ two corrections in the diameter directions of sphere and tube respectively. All functions such as graphics and output data, are integrated into a GUI (Graphics User Interface) based on MATLAB programming, and the GUI is converted to a standalone application which is efficient and convenient, which provided a theoretical basis for robot welding and controlling of this seam weld.

Key words: welding automation; intersection curve of sphere and tube; mathematical model; graphics user interface

Influence of different cooling rates on microstructure of Ti-6Al-4V titanium alloy thermal simulation specimens WANG Jinlin[1], GAN Zhanghua[1], CHEN Yiming[1], XIAO Jianzhong[2] (1. College of Materials Science and Metallurgical Engineering, Wuhan University of Science and Technology, Wu-